SINTECHCOM: Science, Technology and Communication Journal
Vol. 4, No. 3, June 2024, pp. 69-78, DOI: 10.59190/stc.v4i3.262

Novel approach peak tracking method for FBG: Gaussian polynomial technique

Bunga Meyzia[1,*], Tengku Emrinaldi[1], Nadiah Wanara[1], Dwi Hanto[2], Bambang Widyatmoko[2], Agitta Rianaris[2], Mohamad Syahadi[2], Haryana Mohd Hairi[3]
[1]Department of Physics, Universitas Riau, Pekanbaru 28293, Indonesia
[2]Research Center for Photonics, BRIN - KST BJ HABIBIE, South Tangerang 15314, Indonesia
[3]Department of Physics, Universiti Teknologi MARA, Shah Alam 40450, Malaysia

ABSTRACT

This paper presents a novel approach for tracking the peaks in the FBG spectrum using the Gaussian polynomial method. The proposed algorithm involves preprocessing the FBG signal, detecting the peaks, and fitting the peaks with a Gaussian function. The performance of the algorithm is evaluated using both simulated and experimental FBG spectra. This method involves fitting a Gaussian function to the peak of interest and using the fitted parameters to estimate peak height, width, and location. The method is highly accurate and precise and can provide detailed information about peak shape and position, making it effective for tracking complex or overlapping peaks. However, the method can be computationally intensive and may require careful selection of initial parameters to ensure accurate results. Despite these limitations, the Gaussian polynomial method is a powerful tool for peak tracking and analysis in various application.

ARTICLE INFO

Article history:

Received Mar 14, 2024
Revised May 16, 2024
Accepted Jun 18, 2024

Keywords:

Algorithm
FBG Uniform
Fiber Bragg Grating
Gaussian Polynomial
Interrogator

* **Corresponding Author**
E-mail address: bungameyzia@gmail.com

1. INTRODUCTION

The development of optical sensors including fiber Bragg grating (FBG) sensors is very significant in various industrial fields because it has the ability to match electrical sensors such as having high sensitivity, small size but has high resolution to measure wavelength shifts, is not affected by magnetic field and radio frequency interference and has a high signal to noise ratio (SNR) [1-3]. As one of the promising technologies, FBG sensors are commonly used as wavelength reflectors. This is based on spectral filters as the principle of reflection. Light from a broadband source is passed through the FBG, some light will usually reflect narrow wavelengths and other light will be transmitted [4-6].

When light passes through each refractive index region, it will reflect light in each region it passes through. Parameters that can be affected by light reflection are coupling power, spectral angle of reflection and transmission, fiber geometry and the refractive index used [7-10]. When light passes through the fiber, several parameters can be indicated by the FBG spectral, namely the lattice period, excitation conditions, temperature, refractive index changes and fiber length [11-14]. When light with a certain wavelength spreads through the fiber, the Bragg wavelength resulting from the spread depends on the effective refractive index in the core and the lattice period. Intrinsically, both of these parameters depend on temperature and axial stress, so that any modification made to the stress and temperature causes the Bragg wavelength to change. This makes these two parameters one of the characteristics of the FBG [15-18]. There are several ways that can be used to see the results of the FBG spectral monitoring produced. Generally, the system used has two methods, namely a system based on the use of a spectrometer and a broadband source and a laser where the light passed through

can be adjusted and the use of a photodetector [19-22]. The use of this method can generally collect the FBG reflection spectrum so that the wavelength peak can be detected using the wavelength peak tracking algorithm. The systems that can be used are the FBG interrogator system, optical spectrum analyzer (OSA) and tunable laser source (TLS) [23-25].

The use of the FBG sensor multiplexing technique allows the interrogator to track hundreds of signals at the same time, so that the use of algorithms to detect wavelength peaks is faster and more efficient. Several algorithms have been used to detect wavelength peaks such as the spures fitting method, but this algorithm still takes a long time to use, especially when using board processors such as microcontrollers. In addition, the use of maximum algorithms, first order derivatives and the holding method have many shortcomings such as weak anti-noise performance and low accuracy. This study uses curve fitting such as Gaussian, polynomial and the use of centroid algorithms in determining the peak wavelength because this method has high accuracy.

2. FABRICATION THEORY AND FACTORIAL DESIGN

FBG produces a resonance called Bragg wavelength when light is passed from a light source. Optically, FBG acts as a reflective filter where the fiber produces a narrow spectrum while other light is transmitted through the refractive index area. Viewed from the first-order grating diffraction, the Bragg wavelength (λ_B) can be found by [26]:

$$\lambda_B = 2\, n_{eff}\, \Lambda \tag{1}$$

where n_{eff} is the effective refractive index of the fiber optic grating, Λ is the period of refractive index change. The use of a wavelength center with a range of 1520 – 1600 nm, generally uses an effective refractive index value of ≈ 1.5, and the grating period is in the range of 505 – 535 nm. To obtain high accuracy, calibration needs to be done so that the shift in the peak wavelength value does not change significantly. This can be overcome by estimating the use of the f function when the experiment and fabrication are carried out. The use of temperature (T), humidity (H), and strain (ε) variations causes changes in the Bragg wavelength can be seen in:

$$\lambda_B = f(T, H, \varepsilon) \tag{2}$$

The experimental approach to making FBG and calibration can use a three-variable system, namely:

$$y = f\,(x_1, x_2, x_3) \tag{3}$$

where f is an unknown function used for calibration measurements. However, this equation is too common, so the Taylor series expansion is used where:

$$y = a_0 + \sum_{i=1}^{3} a_i x_i + \sum_{i=1}^{3}\sum_{j=1}^{3} a_{ij} x_i x_j + + \sum_{i=1}^{3}\sum_{j=1}^{3}\sum_{k=1}^{3} a_{ijk} x_i x_j x_k + \cdots \tag{4}$$

where y is the response result, x_i is a factor i, a_0 (1 coefficient), a_i (3 coefficients), a_{ij} (9 coefficients where 6 coefficients are free), and a_{ijk} (27 coefficients with 10 free coefficients). All of these coefficients represent the results of the polynomial response where:

$$a_0 = f(0,0,0), a_i = \left.\frac{\partial f}{\partial x_i}\right|_{(0,0,0)}, a_{ij} = \left.\frac{1}{2}\frac{\partial^2 f}{\partial x_i \partial x_j}\right|_{(0,0,0)}, a_i = \left.\frac{1}{3!}\frac{\partial^3 f}{\partial x_i \partial x_j \partial x_k}\right|_{(0,0,0)} \tag{5}$$

This equation is used to monitor humidity using an FBG sensor using a range of temperature and strain. This is a consideration to explain the first-order model by ignoring all parameters that have a power greater than 1 from each variable x_i. Then Equation (4) changes to:

$$y = a_0 + \sum_{i=1}^{n} a_i x_i + \sum_{i=1}^{n}\sum_{j\neq 1}^{n} a_{ij} x_i x_j + a_{123} x_1 x_2 x_3 \tag{6}$$

when $a_{ij} = a_{ji}$, then Equation (6) becomes:

$$y = a_0 + \sum_{i=1}^{n} a_i x_i + \sum_{i=1}^{n} \sum_{j=i+1}^{n} a_{ij} x_i x_j + a_{123} x_1 x_2 x_3 \quad (7)$$

where $a_{ij} = \partial^2 f / (\partial x_i \partial x_j)\big|_{(0,0,0)}$, $i < j$.

When the simulation is carried out and compared with the experiment, using the center point and scale variation, the relationship between:

$$x_i = \frac{x_i - m_i}{\Delta_i} \quad (8)$$

where $m_i = (X_{i,max} + X_{i,min})/2$ is the center value and $\Delta_i = (X_{i,max} - X_{i,min})/2$ is the processing step can be seen. The best point of experimental work is in the ventricle (minimum and maximum values of $X_i = \pm 1$). These values can be seen in Figure 1.

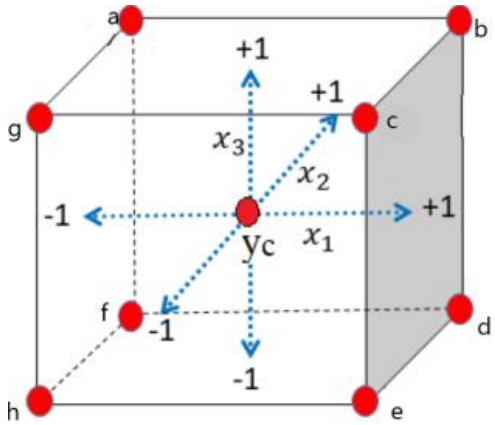

Figure 1. 3-factor design at two levels experimentally.

Figure 1 explains the range of parameters used. The best position is at points a, b, c, d, e, f, g, and h. The mathematical model used is a linear model with first-order interaction. So the normalized Bragg wavelength is:

$$\lambda_B = a_0 + a_H x_H + a_S x_s + a_T x_T + a_{TH} x_T x_H + a_{TS} x_T x_S + a_{HS} x_H x_S + a_{THS} x_T x_H x_S \quad (9)$$

while the unnormalized Bragg wavelength is:

$$\lambda_B = S_0 + S_H \Delta_H + S_S \Delta_s + S_T \Delta_T + S_{TH} \Delta_T \Delta_H + S_{TS} \Delta_T \Delta_S + S_{HS} \Delta_H \Delta_S + S_{THS} \Delta_T \Delta_H \Delta_S \quad (10)$$

where the coefficient value a is interpreted as normalized sensitivity and cross sensitivity. Equation (9) is an important equation for calibrating the sensor, so that the required coefficients can be generated and facilitate simulation. Equation (9) contains 8 unknown a coefficients, then simulated using the matrix in Equation (11):

$$\lambda = \begin{bmatrix} \lambda_a \\ \lambda_b \\ \lambda_c \\ \lambda_d \\ \lambda_e \\ \lambda_f \\ \lambda_h \\ \lambda_g \end{bmatrix}, X = \begin{bmatrix} +1-1 & -1-1 & +1+1 & +1-1 \\ +1+1 & -1-1 & -1-1 & +1+1 \\ +1-1 & +1-1 & -1+1 & -1+1 \\ +1+1 & +1-1 & +1-1 & -1-1 \\ +1-1 & -1+1 & +1-1 & -1+1 \\ +1+1 & -1+1 & -1+1 & -1-1 \\ +1-1 & +1+1 & -1-1 & +1-1 \\ +1+1 & +1+1 & +1+1 & +1+1 \end{bmatrix}, a = \begin{bmatrix} a_0 \\ a_T \\ a_H \\ a_S \\ a_{TH} \\ a_{TS} \\ a_{HS} \\ a_{THS} \end{bmatrix} \quad (11)$$

The cross sensitivity between two variables is marked with variables S_{TH}, S_{HS}, and S_{TS}, while the cross sensitivity for all variables is marked with S_{THS}. This variable gives significant results when the simulation is carried out, so that the points inside the cube can be found using Equation (10).

3. WAVE PEAK DETECTION ALGORITHM

The narrow peaks produced by the reflection filter on the uniform FBG make it possible to fabricate FBGs with various identical FBGs. However, the use of optoelectronic devices such as interrogators, OSA, TLS and InGaAs photodiodes to measure the spectrum of the fabricated FBG produces different wave peaks. This is due to variations in strain and temperature that occur along the lattice area. Several techniques are used to detect wave peaks, namely the direct method, fitting method, and curve fitting.

3.1. Direct Method

This method is the simplest method for detecting reflection peaks without changing the shape. This direct method consists of several methods, namely:

3.1.1. Maximum Value Method

This method is used by looking at the reflectivity peak obtained on the wave using the equation:

$$\lambda_{B,e} = \lambda|_{R(\lambda)=R_{max}} \tag{12}$$

where R_{max} is the maximum reflectivity measured. However, this method is less efficient and less accurate than other methods.

3.1.2. Bandwidth X-dB Method (X-BW)

This method is often implemented on interrogator devices because it has a technique that can be used in the use of wavelengths ($\delta\lambda$ = 1 – 5 pm) (see Figure 2).

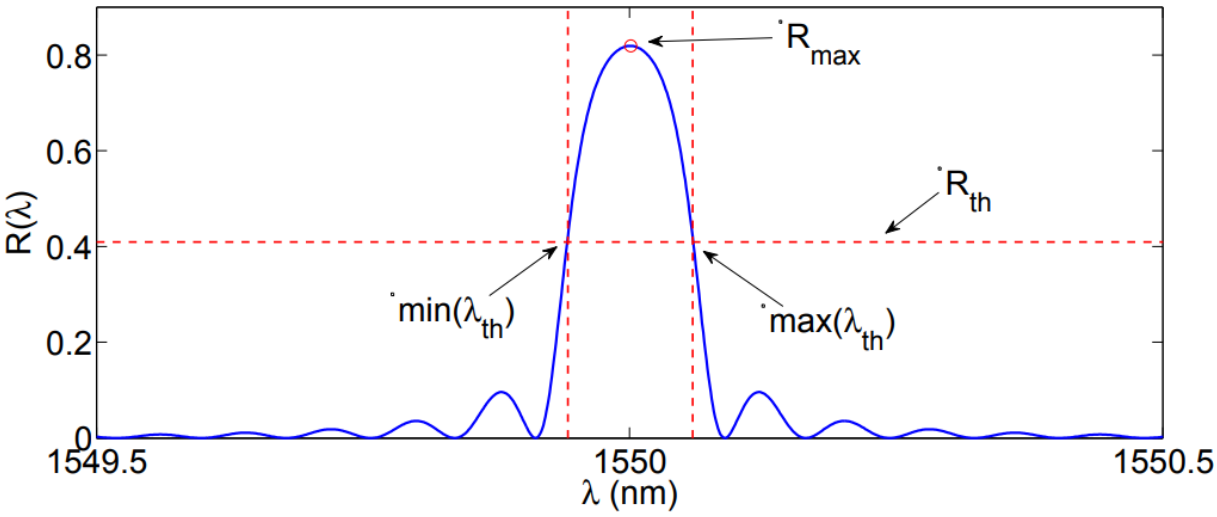

Figure 2. Bandwidth X-DB method image.

The equations used in this method are:

$$R_{th} = \frac{R_{max}}{10log_{10}X} \tag{13}$$

$$\lambda_{B,e} = min\lambda_{(th)} + \frac{max\lambda_{(th)} - min\lambda_{(th)}}{2} \tag{14}$$

where R_{th} is the threshold value that has a spectrum of X dB values at the maximum reflectivity value measured R_{max}.

3.1.3. Centroid Method

The peak of the wave determined from this method is seen from the center of the FBG reflection spectrum. Mathematically, this method is explained by the Equation (15):

$$\lambda_{B,e} = \frac{\sum_0^n \lambda_n * R(\lambda_n)}{\sum_0^n R(\lambda_n)} \tag{15}$$

Empirically, the use of this method depends on the width of the spectral range, so that it can show the estimated wavelength bias against the Bragg wavelength. However, because this method is used to detect waves that match the reference wave, the use of this method is less suitable for use.

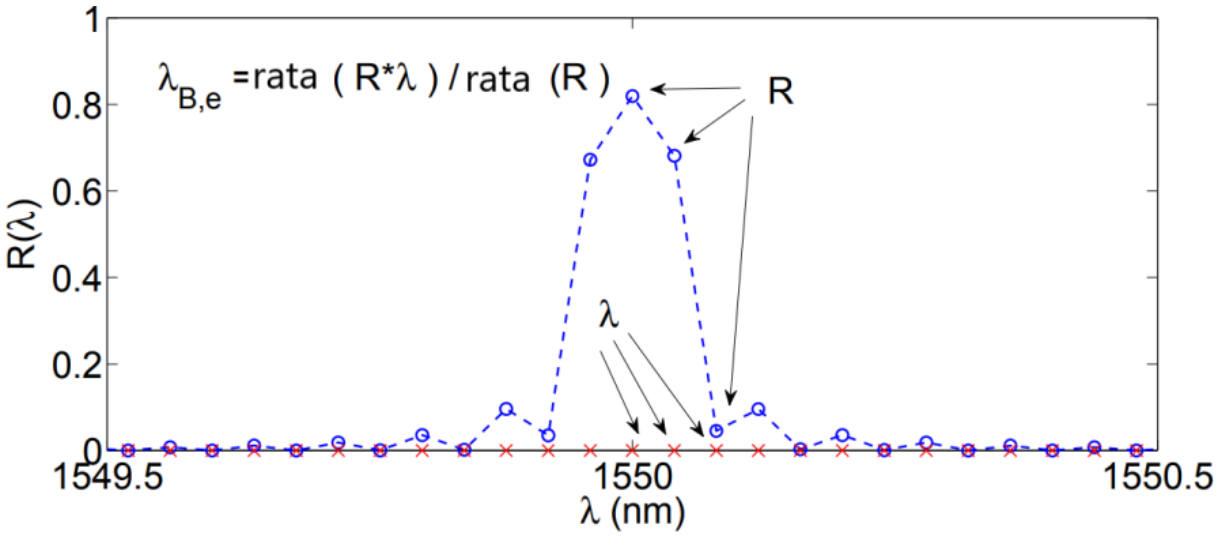

Figure 3. Centroid method image.

3.2. Curve Fitting Method

This method uses a spectrum that is interpolated with several functions to produce the FBG spectrum shape. The techniques used are:

3.2.1. Gaussian Polynomial Method

This technique uses mathematical equations to analyze the FBG reflection spectrum so that the spectrum peak is produced. The functions produced using this method are the peak wavelength, bandwidth and reflectivity. This function is stated in Equation (16):

$$f(x) = A * \frac{\exp(-(x-\mu)^2}{2\sigma^2} \tag{16}$$

where μ is the peak wave, σ is the standard deviation and A is the amplitude. This function is in the form of a symmetrical curve located at the center of the wavelength and its width is determined by the bandwidth.

This method is very suitable for analyzing the spectrum because it can determine accurate parameters such as peak wavelength, bandwidth and reflectivity. This is because the shape of the FBG spectrum is similar to the Gaussian function. In addition, the use of this method is very suitable for use on a lot of data, making it a useful method for characterizing FBG performance. This method is also good for optimizing FBG design. So that it can modify the lattice parameters to achieve the desired performance specifications.

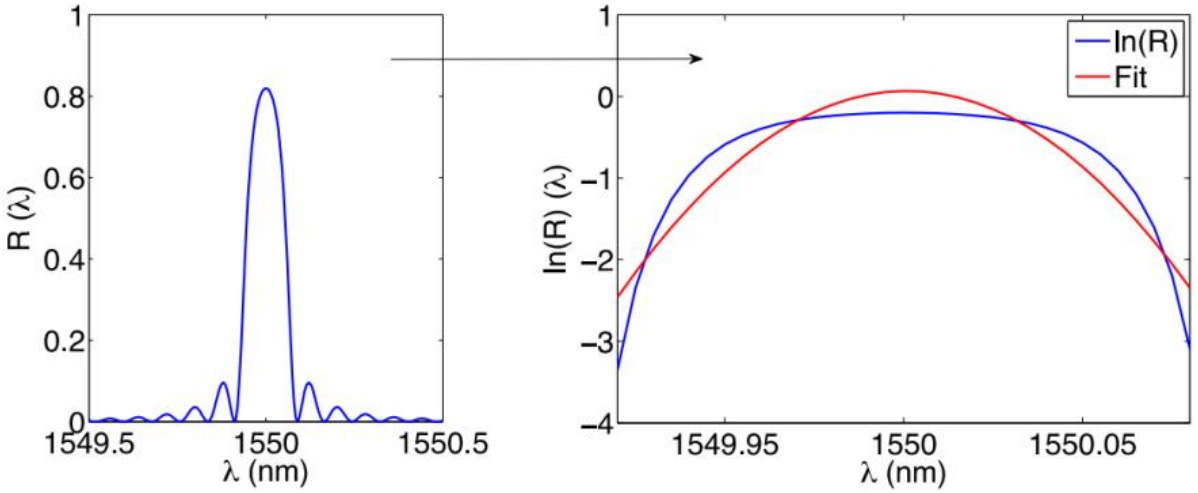

Figure 4. Gaussian method image, the FBG spectrum (left) and the results of using the Gaussian method (right).

4. RESULTS AND DISCUSSIONS

The peak value of the fabricated uniform FBG has a value that varies according to the reflectivity value used. The following are the values and parameters obtained when the FBG was fabricated as shown in Table 1.

Table 1. Reference parameters of uniform FBG values.

Λb (nm)	Bandwidth (nm)	SLSR (dB)	Reflectivity (%)
1549.837	0.13	17.62	10
1549.974	0.147	18.48	30
1549.936	0.176	14.99	50
1549.895	0.216	14.18	70
1549.962	0.284	20.26	90

The peak wavelength values obtained from the FBG fabrication results with reflectivities of 10%, 30%, 50%, 70%, and 90% can be seen in Table 1. These values are then tested through experimental measurements with several instruments such as interrogators and OSA. The measurement results using the interrogator were tested using the Gaussian polynomial method which can be seen in Figure 5. The results obtained can be seen in Table 2.

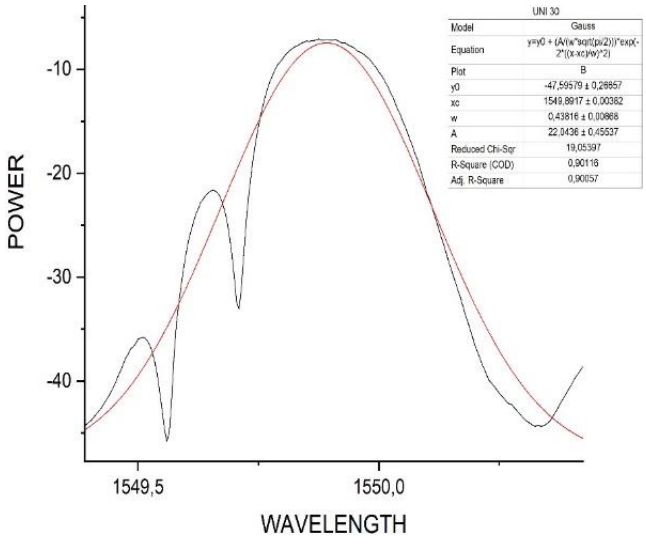

Figure 5. Results of uniform wavelength measurement detection on the interrogator using Gaussian polynomial.

Table 2. Results of interrogator measurement using the Gaussian method.

	UNI 30	UNI 50	UNI 70	UNI 90
w	0.43816 ± 0.00868	0.43819 ± 0.00865	0.43738 ± 0.00861	0.28103 ± 0.00425
R value (Correlation coefficient)	0.9493	0.94969	0.95002	0.97025
A	22.0436	22.03015	21.97552 ± 0.45092	15.54504
Sigma	0.21908	0.2191	0.21869	0.14051
FWHM	0.5159	0.51593	0.51498	0.33089
Peak	1549.8917 ± 0.00382	1549.88847 ± 0.00381	1549.88593 ± 0.00379	1549.86612 ± 0.00199
Reduced Chi-Sqr	19.05397	18.86921	18.71527	9.73961
R square (COD) (Determination coefficient)	0.90116	0.90191	0.90253	0.94138
Adj. R-square	0.90057	0.90132	0.90194	0.94102

Table 2 shows the peak wave value that is different from the reference wavelength caused by the high spectral resolution so that measurements can be made more accurately than the reference value. The peak value measured on a uniform FBG with a reflectivity of 30% is at 1549.8917 and has a difference (Δλ) of about 0.0823 from the reference value of 1549.974. The peak value of a uniform FBG with a reflectivity of 50% is at 1549.88847 and has a difference (Δλ) of about 0.04753 from the reference value of 1549.936. The peak value of uniform FBG with 70% reflectivity is at 1549.88593 and has a difference (Δλ) of around 0.00907. The peak value of uniform FBG with 90% reflectivity is at 1549.86612 and has a difference (Δλ) of around 0.09588 with the reference value of 1549.962. From the results it can be seen that all measurements of FBG peak values experience a wavelength shift due to the influence of the accuracy of the wavelength measurement equipment as the main factor. This accuracy can affect the comparison of the Bragg wavelength with the fabrication results. After using the interrogator, the wavelength detection is continued using OSA. The results were tested using the Gaussian polynomial method which can be seen in Figure 6. The results obtained can be seen in Table 3.

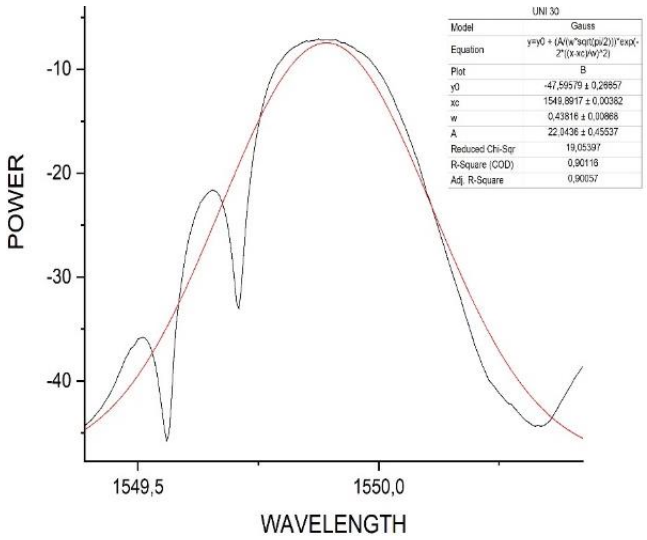

Figure 6. Results of uniform wavelength measurement detection on OSA using Gaussian polynomial.

Table 3 shows the results of FBG characterization using OSA using the Gaussian polynomial method. Table 3 shows that the use of different detectors also makes the peak reflectivity results different. This is because the measurement principles and parameters obtained are different. The Bragg

wavelength value of each FBG that has a variation in reflectivity experiences a difference in wavelength. The peak value of the Bragg wave at a uniform reflectivity of 30% is 1550.00618 nm, 50% reflectivity is at 1549.96749 nm, 70% reflectivity is at 1549.8947 nm, 90% reflectivity is at 1549.9778 nm and reflectivity at a wavelength of 1560 is at 1560.41131 nm. The difference occurs due to several factors such as errors in the fabrication process, environmental factors that affect the grating response and inaccuracies in OSA calibration. Periodic disturbances in the refractive index of the fiber during FBG fabrication will produce several Bragg reflections or gratings that interfere with each other to form a grating spectral response. However, due to the imperfect fabrication process, there is a slight deviation from the desired spectral response so that the fabrication value and the wave value when detected are different.

Table 3. Results of OSA measurement using the Gaussian method.

	UNI 30	UNI 50	UNI 70	UNI 90
w	0.13076 ± 5.62295E-4	0.16488 ± 8.77768E-4	0.19498 ± 0.00116	0.23169 ± 0.00193
R value (Correlation coefficient)	0.99505	0.99235	0.99045	0.98117
A	0.70261 ± 0.00278	1.37833 ± 0.00688	1.85184 ± 0.01045	2.55549 ± 0.00193
Sigma	0.06538	0.08244	0.09749	0.11584
FWHM	0.15395	0.19413	0.22957	0.27279
Peak	1550.00618 ± 2.72E-4	1549.96749 ± 4.20E-4	1549.8947 ± 5.466E-4	1549.9778 ± 9.00E-4
Reduced Chi-Sqr	0.00941	0.04309	0.07978	0.24565
R square (COD) (Determination coefficient)	0.99013	0.98476	0.98099	0.96269
Adj. R-square	0.9901	0.98471	0.98093	0.96258

5. CONCLUSION

This article describes the experimental detection of Bragg wave peaks. Peak detection is very important to analyze and identify reflection peaks in various spectra. This method uses a Gaussian function so that it can produce parameters such as peaks, spectrum widths and reflectivity. The use of this method is an effective approach that has high accuracy so that peak changes can be monitored significantly. This is useful for analyzing spectrum properties. The use of this method also gives good results from several other techniques and can extract more detailed information about the position and shape of the peak. Although effective for detecting complex peaks, this method has limitations such as being less sensitive to noise and signal fluctuations.

REFERENCES

[1] Hikma, N., Saktioto, T., & Soerbakti, Y. (2023). Vibration analysis of diaphragmatic breathing activity using single-mode fiber and fiber Bragg grating. *AIP Conference Proceedings*, **2858**(1).

[2] Zairmi, Y., Basdyo, D., Hairi, H. M., Abd Aziz, M. S., & Abdullah, H. Y. (2022). Inspection of birefringence characteristics to establish single-mode fiber quality. *Science, Technology and Communication Journal*, **2**(3), 91–96.

[3] Peixin, G. A. O., Tao, Y. U., Zhang, Y., Jiao, W. A. N. G., & Jingyu, Z. H. A. I. (2021). Vibration analysis and control technologies of hydraulic pipeline system in aircraft: A review. *Chinese Journal of Aeronautics*, **34**(4), 83–114.

[4] Defrianto, Saktioto, T., Soerbakti, Y., Thoibah, A., Meyzia, B., Syahputra, R. F., Irawan, D., & Hairi, H. (2023). Numerical Investigation of Physical Parameters in Cardiac Vessels as a New Medical Support Science for Complex Blood Flow Characteristics. *Baghdad Science Journal*, **20**(6), 2322–2329.

[5] Animasaun, I. L., Ibraheem, R. O., Mahanthesh, B., & Babatunde, H. A. (2019). A meta-analysis on the effects of haphazard motion of tiny/nano-sized particles on the dynamics and other physical properties of some fluids. *Chinese Journal of Physics*, **60**, 676–687.
[6] Saktioto, T., Defrianto, D., Hikma, N., Soerbakti, Y., Syamsudhuha, S., Irawan, D., Okfalisa, O., Widiyatmoko, B., & Hanto, D. (2022). Airflow vibration of diaphragmatic breathing: model and demonstration using optical biosensor. *TELKOMNIKA (Telecommunication Computing Electronics and Control)*, **21**(3), 667–674.
[7] Zhao, W. M., Wang, Q., Wang, X. Z., Li, X., Jing, J. Y., & Sun, H. Z. (2019). Theoretical and experimental research of lossy mode resonance-based high-sensitivity optical fiber refractive index sensors. *JOSA B*, **36**(8), 2069–2078.
[8] Liu, C., Lü, J., Liu, W., Wang, F., & Chu, P. K. (2021). Overview of refractive index sensors comprising photonic crystal fibers based on the surface plasmon resonance effect. *Chinese Optics Letters*, **19**(10), 102202.
[9] Urrutia, A., Del Villar, I., Zubiate, P., & Zamarreño, C. R. (2019). A comprehensive review of optical fiber refractometers: Toward a standard comparative criterion. *Laser and Photonics Reviews*, **13**(11), 1900094.
[10] Addanki, S., Amiri, I. S., & Yupapin, P. (2018). Review of optical fibers-introduction and applications in fiber lasers. *Results in Physics*, **10**, 743–750.
[11] Erlinda, S., Veriyanti, V., Saktioto, S., & Abdullah, H. Y. (2022). The effect of light waves on polarization mode disperts. *Science, Technology and Communication Journal*, **2**(2), 49–54.
[12] Chadha, U., Bhardwaj, P., Agarwal, R., Rawat, P., Agarwal, R., Gupta, I., Panjwani, M., Singh, S., Ahuja, C., Selvaraj, S. K. and Banavoth, M., Sonar, P., Badoni, B., & Chakravorty, A. (2022). Recent progress and growth in biosensors technology: A critical review. *Journal of Industrial and Engineering Chemistry*, **109**, 21–51.
[13] Saktioto, S., Defrianto, D., Hikma, N., Soerbakti, Y., Irawan, D., Okfalisa, O., Widiyatmoko, B., & Hanto, D. (2022). External perspective of lung airflow model via diaphragm breathing sensor using fiber optic belt. *The 4th Al-Noor International Conference for Science and Technology*, **4**(1), 1014.
[14] Su, T., Liu, N., Lei, D., Wang, L., Ren, Z., Zhang, Q., Su, J., Zhang, Z., & Gao, Y. (2022). Flexible MXene/bacterial cellulose film sound detector based on piezoresistive sensing mechanism. *ACS nano*, **16**(5), 8461–8471.
[15] Nurpadilla, R., Meyzia, B., Saktioto, S., & Fadhali, M. M. (2024). Characteristics of human voice vibrations based on FBG strains. *Science, Technology and Communication Journal*, **4**(2), 33-38.
[16] Maulana, A. M., Ramadhan, K., & Irawan, D. (2023). Analysis of fluid flow in a cylindrical tube using fiber Bragg grating. *Science, Technology and Communication Journal*, **4**(1), 17–22.
[17] Azizah, Y. N., Candra, W., & Fadhali, M. M. (2022). Characteristics of fiber Bragg grating due to temperature changes in honey solution. *Science, Technology and Communication Journal*, **2**(2), 63–68.
[18] Sahota, J. K., Gupta, N., & Dhawan, D. (2020). Fiber Bragg grating sensors for monitoring of physical parameters: A comprehensive review. *Optical Engineering*, **59**(6), 060901–060901.
[19] Fitri, A., Candra, W., & Meyzia, B. (2021). Determination of optical parameters on knee bending of the feet using fiber optic. *Science, Technology and Communication Journal*, **2**(1), 9–14.
[20] Cai, C., Zheng, R., & Luo, J. (2022). Ubiquitous acoustic sensing on commodity iot devices: A survey. *IEEE Communications Surveys & Tutorials*, **24**(1), 432–454.
[21] Ramadhan, K., Irawan, D., & Yupapin, P. (2023). Core multi-layer dispersion on single-mode optical fiber. *Science, Technology and Communication Journal*, **3**(3), 89–94.
[22] Wei, J., Ren, Z., & Lee, C. (2020). Metamaterial technologies for miniaturized infrared spectroscopy: Light sources, sensors, filters, detectors, and integration. *Journal of Applied Physics*, **128**(24).
[23] Mishra, M. & Sahu, P. K. (2023). Fiber Bragg gratings in healthcare applications: A review. *IETE Technical Review*, **40**(2), 202–219.

[24] Maftukhaturrizqoh, O., Wijaya, A. G., Sofia, I. I., Yunianto, M. (2024). Fluid continuity equation simulation: Monitoring fluid reservoir volume in the heart over time. *Science, Technology and Communication Journal*, **4**(2), 45–50.
[25] Basdyo, D., Zairmi, Y., & Yupapin, P. (2022). Non-concentric single-mode optical fiber dispersion. *Science, Technology and Communication Journal*, **3**(1), 7–12.
[26] Hatipoglu, B., Yilmaz, C. M., & Kose, C. (2019). A signal-to-image transformation approach for EEG and MEG signal classification. *Signal, Image and Video Processing*, **13**, 483–490.